PCCP

PAPER

View Article Online
View Journal | View Issue

Check for updates

Cite this: *Phys. Chem. Chem. Phys.*, 2025, **27**, 14410

Robustness of the Floquet topological phase at room temperature: a first-principles dynamics study†

Ruiyi Zhou [a] and Yosuke Kanai*[ab]

Received 14th April 2025,
Accepted 11th June 2025

DOI: 10.1039/d5cp01428j

rsc.li/pccp

Nonadiabatic Thouless pumping of electrons is studied within the framework of topological Floquet engineering, particularly focused on how atomic lattice dynamics affect the emergent Floquet topological phase in *trans*-polyacetylene under the driving electric field. Following the approach in a previous study [R. Zhou *et al.*, *J. Phys. Chem. Lett.*, 2021, **12**, 4496], real-time time-dependent density functional theory and Ehrenfest dynamics simulations were used to investigate the extent to which the number of pumped charges remains equal to the topological invariant, the winding number, when the temperature effect of ions and the dynamical coupling of electrons and ions are taken into account. Our theoretical work shows that the Floquet topological phase remains intact but the condition on the driving field necessary for observing the topological phase becomes more limiting.

Open Access Article. Published on 13 June 2025. Downloaded on 12/6/2025 9:53:45 AM.
This article is licensed under a Creative Commons Attribution 3.0 Unported Licence.

1. Introduction

An earliest realization of how the topological characteristics of a Hamiltonian govern certain dynamical properties came from Thouless when he discussed the quantized pumping phenomenon in 1983.[1] By studying one-dimensional quantum-mechanical particle transport in a slow varying potential, he showed that the quantization of the number of transported quantum particles stems from the topology of the underlying Hamiltonian. Under adiabatic evolution (*i.e.* instantaneous eigenstates of Hamiltonian), the particle current in a one-dimensional system is determined by a topological quantity known as the winding number when the Hamiltonian is periodic in time. For topological materials, the winding number can take a non-zero integer value while it is zero for normal/trivial insulators. In recent years, Thouless pumping has been demonstrated experimentally in various systems[2–5] including an ultracold Fermi gas[6] and ultracold atoms in an optical lattice.[7] Various theoretical studies[8–11] have employed model Hamiltonians such as the Rice-Mele model[12] and the description of topological pumping has often assumed complete adiabaticity of Hamiltonian evolution. At the same time, studies of nonadiabatic effects on Thouless pumping have appeared in the literature.[13–15] A particularly notable development in recent years has been the idea of the so-called topological Floquet engineering, in which one uses a time-periodic external field to induce a topological phase in the driven system that is otherwise a trivial insulator.[16,17] Briefly, in a Floquet system, the time-dependent Hamiltonian satisfies $\hat{H}(t+T)=\hat{H}(t)$ and an effective time-independent Hamiltonian can be defined from the time evolution operator. One can then apply the topological description analogously to this effective Hamiltonian. Under certain conditions on the driving field, the Floquet topological phase, in which the winding number is a non-zero integer, can emerge. At the same time, unlike for the equilibrium cases, the robustness of such a topological phase is not guaranteed.[17]

Increasing efforts have been devoted to developing a molecular-level understanding of topological materials from the perspective of chemistry,[18–21] which would open up the field for further exploration with a more intuitive viewpoint based on the arrangement of atoms. In our previous work,[22] we have demonstrated nonadiabatic Thouless pumping of electrons in *trans*-polyacetylene under a driving electric field using first-principles theory in the framework of Floquet engineering. By exploiting the gauge invariance of the quantum dynamics in terms of minimal particle–hole excitations,[23] the topological pumping of electrons can also be understood as a cyclic transition among the bonding and antibonding orbitals. Having connected the topological invariant to the chemical bonding concepts,[22] we further demonstrated molecular-level control on the emergence of the Floquet topological phase, presenting exciting possibilities of the intuitive molecular-level engineering for such an exotic topological phase.[24] At the same time, the feasibility of observing Floquet topological pumping at room temperature still remains a practical open question. In this work, we investigate the interplay between the electronic current and the lattice dynamics of atoms on the Floquet topological phase using Ehrenfest dynamics simulation based on real-time time-dependent density functional theory (RT-

[a] *Department of Chemistry, University of North Carolina at Chapel Hill, Chapel Hill, North Carolina 27514, USA. E-mail: ykanai@unc.edu*
[b] *Department of Physics and Astronomy, University of North Carolina at Chapel Hill, Chapel Hill, North Carolina 27514, USA*

† Electronic supplementary information (ESI) available. See DOI: https://doi.org/10.1039/d5cp01428j

This journal is © the Owner Societies 2025

Open Access Article. Published on 13 June 2025. Downloaded on 12/6/2025 9:53:45 AM. This article is licensed under a Creative Commons Attribution 3.0 Unported Licence.

TDDFT). Additionally, we examine the impact of thermal fluctuations in the atomic lattice on the Floquet topological phase by performing RT-TDDFT calculation with first-principles molecular dynamics simulation.

2. Computational details

We examined several exchange–correlation (XC) functionals by calculating the equilibrium geometry of *trans*-polyacetylene as shown in Table 1. Popular XC approximations such as GGA: PBE,[25] meta-GGA:SCAN,[26] and hybrid-GGA:PBE0[27] have not yielded Peierls distortion.[28] This failure is primarily due to self-interaction errors that lead to an over-delocalization of electrons, incorrectly favoring an undistorted structure. In contrast, the SCAN0 approximation,[29] which incorporates 25% exact exchange within a meta-GGA framework, correctly predicts the Peierls distortion, yielding bond lengths in good agreement with experimental data.[30] The accurate representation of bond length alternation is necessary here because these structural details govern the electronic structure and, consequently, the material's electrical conductivity properties. Inaccuracies in bond lengths, as seen with the other XC approximations, would indirectly lead to erroneous predictions of these key characteristics. Therefore, we employ the SCAN0 XC functional for examining lattice dynamical effects in our study.[31] To simulate *trans*-polyacetylene at room temperature (300 K), we performed first-principles molecular dynamics (FPMD) simulations using the SCAN0 XC functional with the FHI-aims code.[32,33] We employ the tier 2 numeric atom-centered orbital (NAO) basis set.[33] FPMD simulations were carried out in the NVT ensemble at 300 K for 4 picoseconds, employing a Nose–Hoover thermostat[34,35] with a thermostat frequency of 1600 cm^{-1}.[36] The FPMD time step of 0.5 femtoseconds was used.

In order to study the Floquet topological phase by simulating nonequilibrium electron dynamics, we perform real-time time-dependent density functional theory (RT-TDDFT)[37–39] and Ehrenfest dynamics[23] based on RT-TDDFT. The mean-field approximation inherent in Ehrenfest dynamics for coupled electron–ion systems imposes limitations on the description of certain energy exchange phenomena, such as Joule heating.[40,41] However, the characteristic timescale of the Floquet topological pump under investigation (approximately several femtoseconds) is significantly shorter than the time required to reach the detailed balance conditions (typically hundreds of femtoseconds to picoseconds or longer). Therefore, we posit that Ehrenfest dynamics provides a sufficient framework for describing the pertinent physics in this study. For Ehrenfest dynamics simulations, we use the Qb@ll branch[42–46] of the Qbox code[47] within the plane-wave pseudopotential (PW-PP) formalism.[48] All atoms were represented by Hamann–Schluter–Chiang–Vanderbilt (HSCV) norm-conserving pseudopotentials,[49,50] with a plane-wave cutoff energy of 40 Ry for the Kohn–Sham (KS) orbitals. For integrating the time-dependent Kohn–Sham equation, we employed the enforced time-reversal symmetry (ETRS) integrator[51] in the maximum localized Wannier function (MLWF) gauge,[52] and we used an integration step size of 0.1 a.u. For the Ehrenfest dynamics simulation, atomic positions were also updated at a time interval of 0.1 a.u. for each integration step. The electric field $\boldsymbol{E}(t) = \boldsymbol{A}\sin\left(\frac{2\pi}{T}t\right)$ was applied as the driving field, and we considered the time periodicity T of 50–200 a.u. and the field amplitude $|\boldsymbol{A}|$ range of 1.0–6.0 $\times 10^{-3}$ a.u. with the uniform sampling intervals of 25 a.u. and 1.0 $\times 10^{-3}$ a.u., respectively. Note that the time-dependent electric field was applied in the length gauge using the scalar potential in the KS Hamiltonian.[46,52] For all simulations, a 55-atom simulation supercell, consisting of 11 C–C monomer units along the x-axis, was employed under the periodic boundary conditions (51.32 × 15.0 × 15.0 Bohr), and the Γ-point approximation for Brillouin zone integration was adopted as done in previous work.[22,24] The comparison between the FHI-aims and Qb@ll codes is provided in Table S1 in the ESI.†

Table 1 Comparison of carbon–carbon bond lengths of the optimized equilibrium structures using several exchange–correlation (XC) functionals, together with the experimental values reported in ref. 30

XC functional	C–C bond length (Angstrom)	C=C bond length (Angstrom)	Peierls distortion
PBE	1.396	1.396	No
SCAN	1.387	1.387	No
Hartree Fock	1.332	1.460	Yes
PBE0	1.393	1.393	No
SCAN0	1.357	1.419	Yes
Experiment	1.36	1.44	Yes

3. Results and discussion

We study two different aspects of the influence of atomic lattice dynamics on the nonadiabatic Thouless pumping of electrons. We examine how the quantum dynamics of electrons can induce the atomic lattice dynamics and potentially degrade the intricated nature of the topological pumping even at 0 K. We performed this by taking into account the nonadiabatic coupling between electrons and classical nuclei in the Ehrenfest dynamics simulation. In this simulation, an initial temperature of 0 K is used for the lattice. Secondly, we examine the thermal fluctuations of the atomic lattice on the quantum dynamics of electrons. Because of the vastly different relevant timescale differences (*i.e.* femto-seconds for the pumping dynamics *vs.* picoseconds for the lattice dynamics), we simple take snapshots from FPMD simulations at 300 K and perform RT-TDDFT on these static structures.

3.1. Coupling between lattice dynamics and electron transport

As shown in our previous work,[22,24] the (time-) integrated current, $Q(T)$, can be calculated *via* time-dependent maximally localized Wannier functions (MLWFs), $w_i(r, t)$, as follows:[22]

$$Q(T) = L^{-1}\sum_{i}^{\mathrm{Occ.}}[\langle w_i(T)|\hat{r}|w_i(T)\rangle - \langle w_i(t=0)|\hat{r}|w_i(t=0)\rangle] \quad (1)$$

where the position operator $\hat{r}$ is defined according to the formula given by Resta for extended periodic systems[53] and L

Open Access Article. Published on 13 June 2025. Downloaded on 12/6/2025 9:53:45 AM.
This article is licensed under a Creative Commons Attribution 3.0 Unported Licence.

is the lattice length of the unit cell. In short, the integrated current $Q(T)$ is equal to the number of the geometric centers of the MLWFs (*i.e.* Wannier centers) transported over time T.[54,55] In the context of Floquet theory, the initial state must return to the same Hilbert subspace of the Floquet operator after a driving period. The Kohn–Sham Hamiltonian depends on the time-dependent electron density even when the adiabatic approximation is adapted for the exchange–correlation potential.[56,57] Therefore, the Hamiltonian is time-periodic (*i.e.* Floquet theory $\hat{H}(t+T) = \hat{H}(t)$ is applicable) only if the initial electron density is recovered after each driving cycle is completed. We can quantify the extent to which the Floquet condition is satisfied by calculating the determinant of the overlap matrix $S_{ij} = \langle\psi_i(0)|\psi_i(T)\rangle$, between the initial time-dependent Kohn–Sham (TD-KS) orbitals and those after one driving cycle has finished, as shown in Fig. 1, and also discussed in ref. 22. When the Floquet condition (*i.e.* $|\det(\boldsymbol{S})| = 1$) is satisfied, the integrated current, $Q(T)$, is equal to the winding number, W, an integer.[22,24] The topological phase is identified as having a non-zero integer value of W while the $W = 0$ phase indicates the trivial insulator phase.

In the RT-TDDFT simulation, the lattice (atomic nuclei) is held fixed in time at equilibrium positions. In the Ehrenfest dynamics simulation, the atomic nuclei are allowed to respond to the time-dependent movement of electrons in the system according to the instantaneous Coulomb force on the atomic nuclei. The atomic nuclei thus move and respond to the non-equilibrium electron density and to the external driving field. Fig. 1 (top) shows the extent to which the Floquet condition is satisfied; the red-colored areas (indicating $|\det(\boldsymbol{S})| > 0.95$) decrease when the dynamical coupling between the electrons and atomic nuclei is taken into account as in the Ehrenfest dynamics simulation. As perhaps expected, the higher the driving field amplitude is the more differences we tend to observe between RT-TDDFT and Ehrenfest dynamic simulations.

Fig. 1 (bottom) shows $Q(T)$ per monomer as a function of the driving field amplitude and period. As can be seen, the Floquet topological phase remains largely intact even with the dynamical coupling between electrons and atomic nuclei. For the driving field amplitude above $|\boldsymbol{A}| = 2 \times 10^{-3}$ a.u. (1 a.u. $\approx$ 5.1422 V Å^{-1}), the RT-TDDFT simulation shows that the topological phase is observed when the Floquet condition is satisfied. With the Ehrenfest dynamics simulation, the lattice movement somewhat makes it more difficult to satisfy the Floquet condition; a notable change is observed for $T = 150$ a.u./$|\boldsymbol{A}| = 5 \times 10^{-3}$ a.u. (as marked by the red square box in Fig. 1 (bottom)). The Floquet topological phase ($W = 1$) can be found here as opposed to the trivial phase in the RT-TDDFT simulation. With the dynamical coupling of electrons and atomic nuclei in Ehrenfest dynamics, $|\mathrm{Det}(\boldsymbol{S})|$ is only 0.93, and the Floquet condition is not lifted appreciably. The integrated current gives $Q(T) = 0.92$, and it deviates noticeably

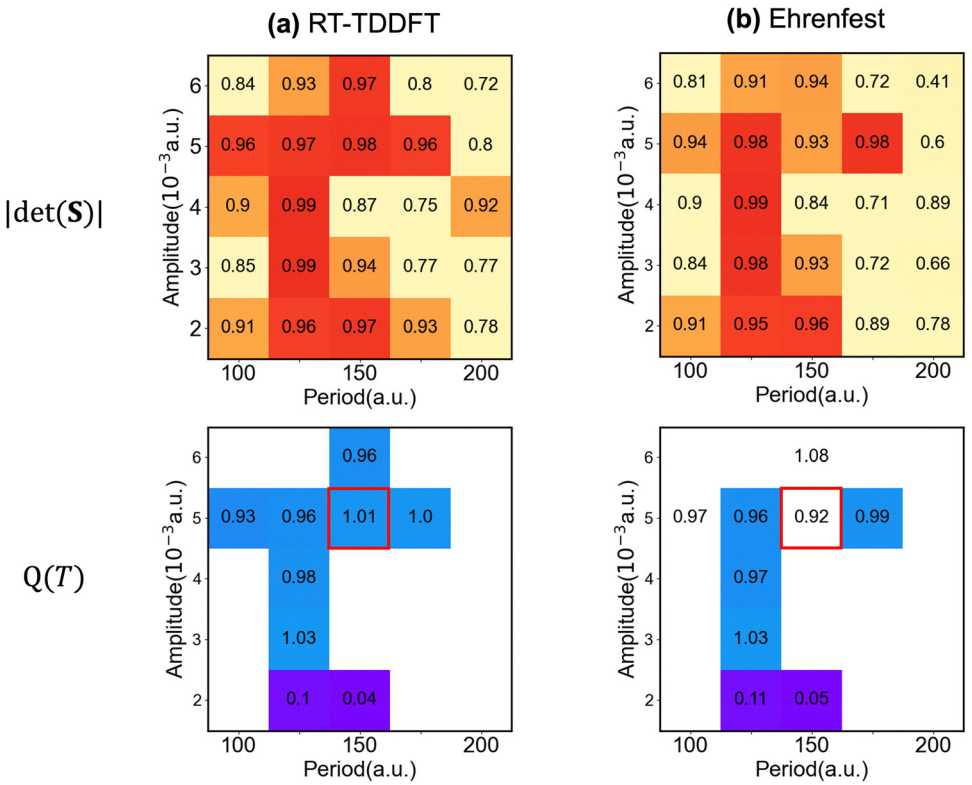

Fig. 1 (top) The determinant of the overlap matrix, $\boldsymbol{S}$, between the initial and final TD-KS states in a single driving cycle and (bottom) the time-integrated current over a single driving cycle $Q(T)$ plotted as a function of the driving electric field amplitude $|\boldsymbol{A}|$ and the period T for (a) RT-TDDFT and (b) Ehrenfest dynamics. The colors indicate the value of $|\det(\boldsymbol{S})|$ in top figures: red (>0.95), orange (0.90–0.95), and yellow (<0.90). In bottom figures, the purple and blue colors indicate the assignment of the trivial and topological phases, respectively. The red box indicates the specific driving field for which the electron dynamics were analysed in detail (see the main text).

 This journal is © the Owner Societies 2025

Open Access Article. Published on 13 June 2025. Downloaded on 12/6/2025 9:53:45 AM.
This article is licensed under a Creative Commons Attribution 3.0 Unported Licence.

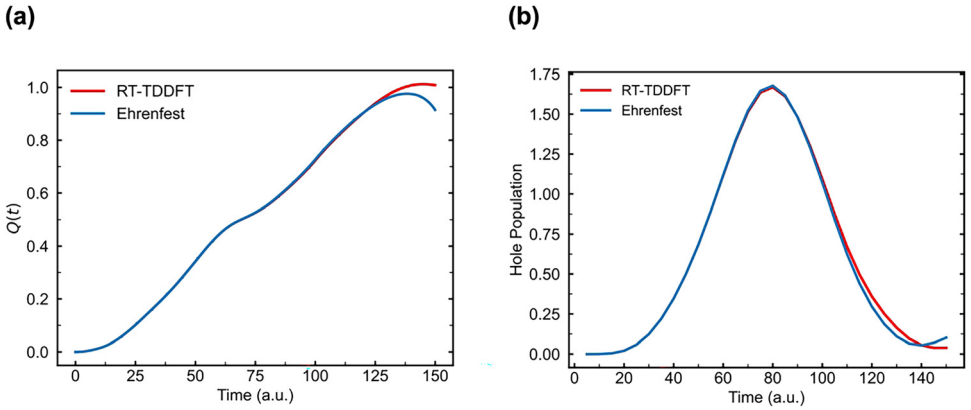

Fig. 2 Electron dynamics from RT-TDDFT and Ehrenfest dynamics simulations of *trans*-polyacetylene with the driving field of T = 150 a.u./$|\boldsymbol{A}|$ = 5 × 10^{-3} a.u. (as marked by the red box in Fig. 1). (a) Time-integrated current $Q(t)$ as a function of time t. (b) Time-dependent hole occupation, calculated by projecting the time-dependent orbitals onto the equilibrium Kohn–Sham eigenstates.

from the integer value of $Q(T)$ = 1 as one would expect for the topological phase even if one considers errors from numerical simulations. The difference becomes more evident when $Q(t)$ is plotted as a function of time as done in Fig. 2(a). This quantity can be conveniently calculated using the Wannier centers as in eqn (1) from the RT-TDDFT and Ehrenfest dynamics simulations. Both simulations show identical behavior up until the last t = 25 a.u. However, for the Ehrenfest dynamics, the $Q(t)$ value starts to decrease, indicating that the transport direction of the C–C and C=C Wannier functions reverses to the opposite direction at t = 125–150 a.u. Then, the time-dependent electron density does not evolve back to the initial state after a single driving cycle, leaving some electrons excited after the periodic time, T (see Fig. 2(b)); the Floquet condition is not satisfied because the single-particle KS Hamiltonian is dependent on the time-dependent density.

3.2. Thermal fluctuations of the lattice on electron transport

Let us now discuss the impact of thermal fluctuations of atoms at room temperature on the Floquet topological phase. In order to sample representative geometries, the first-principles molecular dynamics (FPMD) simulation was performed in the electronic ground state at 300 K for 4 picoseconds. FPMD trajectories show fluctuations in both C–C and C=C bond lengths. At the same time, the analysis of the Wannier functions shows that the alternating bonding pattern, resulting from the Peierls instability, is consistently observed throughout the FPMD simulation. To quantify the extent of the Peierls distortion effect,[28] we employ a collective variable, called the bond length alternation (BLA)[58] index. The BLA is defined as the averaged bond length differences between the C–C and C=C bonds

$$\mathrm{BLA} = \frac{1}{N}\sum_{i=1}^{N}\left(r_i^{\mathrm{C=C}} - r_i^{\mathrm{C-C}}\right)$$

where N represents the number of unit cells in the simulation supercell. $r_i^{\mathrm{C=C}}$ and $r_i^{\mathrm{C-C}}$ are the lengths of the carbon–carbon double bond and the carbon–carbon single bond in the i^{th} unit cell, respectively. We considered only the absolute value of BLA due to the inversion symmetry of *trans*-polyacetylene although BLA can take negative values.[58] BLA is a geometric measure of conjugated polymers, and other studies have shown that various electronic[58–60] and optical[61,62] properties can be rationalized in terms of the BLA value. To better establish the relationship between the BLA index and the Peierls distortion in *trans*-polyacetylene at the electronic structure level, the maximally localized Wannier functions (MLWF) are calculated on several selected structures from the FPMD trajectory. Fig. 3 shows how the average spread values of the MLWFs associated with C=C double bonds are correlated with the BLA value. The dashed vertical line indicates the equilibrium structure at 0 K. C=C bonds tend to become, on average, more delocalized with the decreasing BLA value while C–C bonds remain largely unaffected. While the average MLWF spreads show a rather large standard deviation for the double bonds, as indicated by the error bars in

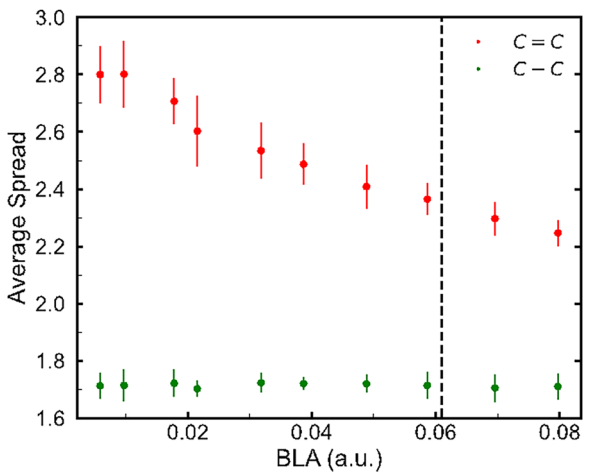

Fig. 3 Average spread values of C=C (red) and C–C (green) maximally localized Wannier functions (MLWFs) in the electronic ground state for structures with different bond length alternation (BLA) values. The structures are taken from the trajectory of the FPMD simulation of *trans*-polyacetylene at 300 K. The vertical dashed line represents the BLA value of the equilibrium (0 K) structure. The error bars indicate the standard deviations among the MLWFs for each bond type.

Open Access Article. Published on 13 June 2025. Downloaded on 12/6/2025 9:53:45 AM.
This article is licensed under a Creative Commons Attribution 3.0 Unported Licence.

Fig. 3, a clear distinction between the double and single bonds can be made for all structures with various BLA values, indicating that the electronic conjugation remains intact even at room temperature.

The RT-TDDFT calculation was performed on four selected structures with different BLA values from the FPMD simulation, as shown in Fig. 4. The Floquet topological phase can be observed in all four cases with the driving field period of approximately 100–150 a.u., which aligns well with our earlier findings.[22,24] At the same time, the extent to which the topological phase is present is highly dependent on the driving field amplitude and the period (see Fig. 4 top). Due to the dynamical disruption to the periodicity of the otherwise perfectly repeating polymer units caused by thermal fluctuations (see Fig. 3), satisfying the Floquet condition with the external driving field becomes more restrictive. Even when the Floquet condition is satisfied, whether the trivial phase ($W = 0$) or the topological phase ($W = 1$) exists is very sensitive to the driving field conditions, strongly varying with the BLA value. For instance, for structure A with a small BLA value of 0.010, not only it is more difficult to have the Floquet condition satisfied but also the emergence of the topological phase is highly dependent on the driving field, particularly with respect to the period of the driving field. In experiments performed at room temperature, all these structural variations with different BLA values would exist and thus finding the driving field conditions under which the Floquet topological phase is observed at all times is likely difficult.

To gain a deeper insight into the quantum dynamic behavior underlying the Floquet topological pump, we discuss two specific conditions for the driving field: $T = 125$ a.u./$|\boldsymbol{A}| = 2 \times 10^{-3}$ a.u. (the pink square in Fig. 4) and $T = 150$ a.u./$|\boldsymbol{A}| = 2 \times 10^{-3}$ a.u. (the orange square in Fig. 4). With $T = 125$ a.u./$|\boldsymbol{A}| = 2 \times 10^{-3}$ a.u., the Floquet topological phase is observed for structures A (BLA = 0.010) and B (BLA = 0.032) while the trivial phase (*i.e.* $W = 0$) is found for structures C (BLA = 0.049) and D (BLA = 0.080) as shown in Fig. 4. Fig. 5 shows the number of transported charges $Q(t)$ as a function of time for all these driving conditions for the four structures. With the driving field of $T = 125$ a.u./$|\boldsymbol{A}| = 2 \times 10^{-3}$ a.u. (Fig. 5(a)), both structures A and B yield $Q(T) = 1$, exhibiting the topological phase although their corresponding quantum dynamics show notable differences. In structure B, $Q(t)$ shows a continuous increase, reaching a value of 1.026 electrons at the end of the single driving cycle. In contrast, for structure A, the current reverses its direction at around $t = 110$ a.u. such that $Q(t)$ decreases before reaching the value of 1.028 electrons at the end of the driving cycle. For structures C and D, the current direction more or less follows the direction of the driving electric field and thus $Q(t)$ is diminishingly small after the period T.

With the driving field of $T = 150$ a.u./$|\boldsymbol{A}| = 2 \times 10^{-3}$ a.u. (Fig. 5(b)), the Floquet topological phase is observed for structures B and C while the trivial phase is found for structure D. Even accounting for some numerical errors in the simulation, the Floquet condition is not satisfied for structure A and $Q(T)$ is

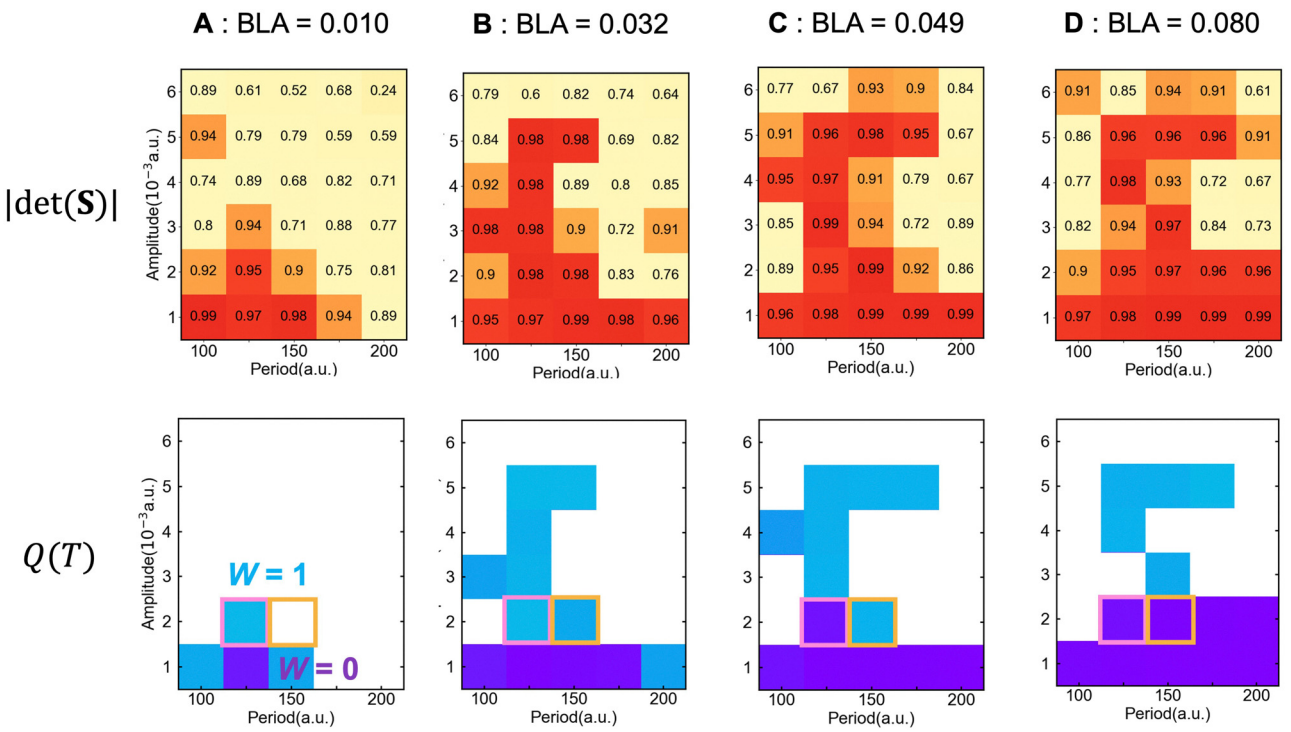

Fig. 4 (top) Time-integrated current over one driving cycle $Q(T)$, and (bottom) the determinant of the overlap matrix, $\boldsymbol{S}$, between the initial and final TD-KS states in a single driving cycle. These values are plotted as a function of the driving electric field amplitude $|\boldsymbol{A}|$ and the time period T for the structures (A)–(D) with various BLA values. These structures are taken from FPMD simulation of *trans*-polyacetylene at 300 K. The white (colorless) areas in the top plot represents that the Floquet condition is not satisfied. The pink ($T = 125$ a.u. and $|\boldsymbol{A}| = 2 \times 10^{-3}$ a.u.) and orange ($T = 125$ a.u. and $|\boldsymbol{A}| = 2 \times 10^{-3}$ a.u.) boxes indicates the specific conditions for which the underlying electron dynamics were investigated in detail as discussed in the main text.

 This journal is © the Owner Societies 2025

Open Access Article. Published on 13 June 2025. Downloaded on 12/6/2025 9:53:45 AM.
This article is licensed under a Creative Commons Attribution 3.0 Unported Licence.

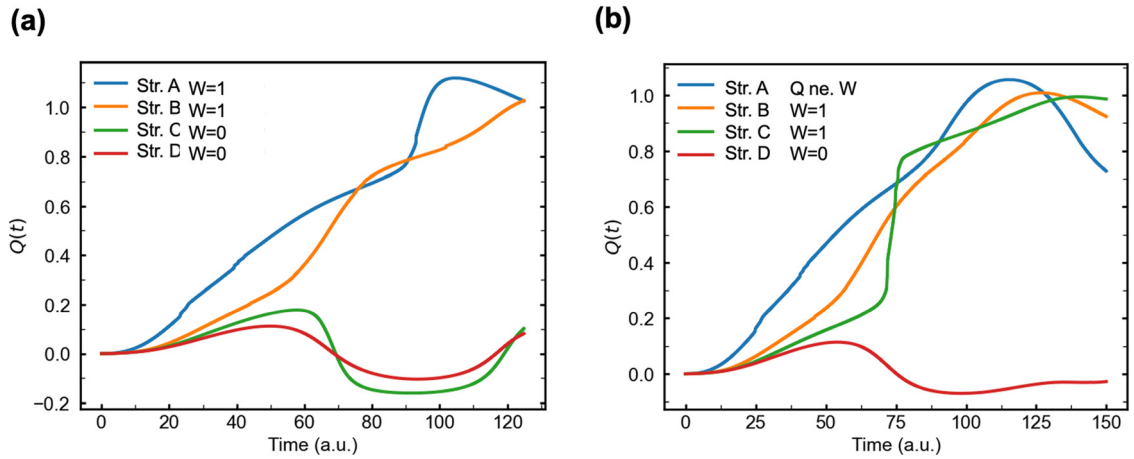

Fig. 5 Time-integrated current as a function of time, $Q(t)$, of *trans*-polyacetylene for the structures of various BLA values with the driving field of (a) T = 125 a.u./$|\boldsymbol{A}|$ = 2 × 10^{-3} a.u. (as marked by the pink square box in Fig. 4) and (b) T = 150 a.u./$|\boldsymbol{A}|$ = 2 × 10^{-3} a.u. (as marked by the orange square box in Fig. 4).

0.73 electrons. Unlike for structure A, structures B and C both largely satisfy the Floquet condition given the same criterion based on the $|\det(\boldsymbol{S})|$. While they tend to exhibit the Floquet topological phase instead of the trivial phase, the degree to which the $Q(T)$ value is close to the integer value of one is noticeably less for structure C; the $Q(T)$ value for structures B and C is 0.99 and 0.92, respectively (see the ESI†). For these structures taken from the room temperature FPMD simulation, the periodicity is not perfectly satisfied and noticeable deviations of $Q(T)$ from $Q(T) = W = 1$ can be anticipated, as discussed earlier. In Fig. 5, another notable feature is the abrupt jump in $Q(t)$ for structure C around t = 75 a.u., and such quantum tunnelling-like behavior has been discussed previously.[23,52] If computational resources were not a factor in these highly demanding RT-TDDFT simulations, one would ideally calculate the ensemble average of $Q(t)$ to model experiments at room temperature. Fig. 5, even with only four representative geometries, shows that such an ensemble-average $\langle Q(t)\rangle$ would not yield the topological phase behavior at 0 K (*i.e.* an integer value at $t = T$) even for the most likely/favorable driving field condition (T = 125 a.u./$|\boldsymbol{A}|$ = 2 × 10^{-3} a.u. (Fig. 5(a))).

Finally, the results here show that bond length alternation (BLA) is an effective geometric parameter for the emergence and characteristics of the Floquet topological phase. As the BLA value decreases, the weakening Peierls distortion leads to electron delocalization within the conjugated chain. In the delocalization limit with BLA = 0, the system becomes metallic with no Peierls distortions. As conveniently seen using the Su-Schrieffer-Heeger model of Peierls instability,[63] a topological phase is precluded in such a gapless metallic system even with an external driving field. At elevated temperatures, thermal fluctuations are more likely to dynamically disrupt the delicate electronic ordering that is required for the topological phase since the geometries with low BLA values are more accessible.

4. Conclusions

Building on the previous work,[22,24] we examined the robustness of the Floquet topological phase in *trans*-polyacetylene with respect to the atomic lattice movement using first-principles simulation. In particular, the effect of atomic lattice dynamics on the Floquet topological phase was investigated by performing Ehrenfest dynamics simulation in which atoms respond to the electronic current. Secondly, we investigated how atomic lattice distortion at room temperature could affect the presence of the Floquet topological phase by performing RT-TDDFT calculations on selected geometries from a separate FPMD simulation at room temperature. When the dynamical coupling between electrons and atomic nuclei is included as in Ehrenfest dynamics simulation, it becomes somewhat more difficult to satisfy the Floquet conditions although the topological phase is largely intact. Additionally, we examined the impact of thermal fluctuations in the atomic lattice on the Floquet topological phase. The bond length alternation (BLA) index was used to quantify the degree of Peierls distortion in terms of the carbon–carbon single and double bonds. The sensitivity of the topological phase to the driving field varies substantially with the BLA value. Therefore, finding the necessary driving field magnitude and period for inducing the Floquet topological phase would be challenging at room temperature in experiments. In this theoretical work, the nuclear quantum fluctuation, as often represented by Wigner distribution, in the Floquet topological phase was not considered. Such a nuclear quantum effect could introduce additional challenges for observing the Floquet topological phase even at low temperatures, and it will be studied in future studies. Finally, the exchange–correlation (XC) approximation in the first-principles simulation was found to have a great impact on the prediction of the Peierls distortion for *trans*-polyacetylene. Improving XC approximation continues to be of great practical importance and such efforts continue to be necessary in the community.

Conflicts of interest

There are no conflicts to declare.

Open Access Article. Published on 13 June 2025. Downloaded on 12/6/2025 9:53:45 AM. This article is licensed under a Creative Commons Attribution 3.0 Unported Licence.

Data availability

The data supporting this article have been included as part of the ESI.†

Acknowledgements

This work was supported by the National Science Foundation under Award No. CHE-1954894 and OAC-2209858. We thank the Research Computing at the University of North Carolina at Chapel Hill for providing computational resources.

References

1 D. J. Thouless, Quantization of Particle Transport, *Phys. Rev. B: Condens. Matter Mater. Phys.*, 1983, **27**, 6083–6087.
2 W. Ma, L. Zhou, Q. Zhang, M. Li, C. Cheng, J. Geng, X. Rong, F. Shi, J. Gong and J. Du, Experimental Observation of a Generalized Thouless Pump with a Single Spin, *Phys. Rev. Lett.*, 2018, **120**, 120501.
3 A. Cerjan, M. Wang, S. Huang, K. P. Chen and M. C. Rechtsman, Thouless Pumping in Disordered Photonic Systems, *Light: Sci. Appl.*, 2020, **9**, 1–7.
4 A.-M. Guo, P.-J. Hu, X.-H. Gao, T.-F. Fang and Q.-F. Sun, Topological Phase Transitions of Thouless Charge Pumping Realized in Helical Organic Molecules with Long-Range Hopping, *Phys. Rev. B*, 2020, **102**, 155402.
5 Y. Zhang, Y. Gao and D. Xiao, Topological Charge Pumping in Twisted Bilayer Graphene, *Phys. Rev. B*, 2020, **101**, 041410.
6 S. Nakajima, T. Tomita, S. Taie, T. Ichinose, H. Ozawa, L. Wang, M. Troyer and Y. Takahashi, Topological Thouless Pumping of Ultracold fermions, *Nat. Phys.*, 2016, **12**, 296.
7 M. Lohse, C. Schweizer, O. Zilberberg, M. Aidelsburger, I. Bloch and A. Thouless, Quantum Pump with Ultracold Bosonic Atoms in an Optical Superlattice, *Nat. Phys.*, 2016, **12**, 350–354.
8 A. Hayward, C. Schweizer, M. Lohse, M. Aidelsburger and F. Heidrich-Meisner, Topological Charge Pumping in the Interacting Bosonic Rice-Mele Model, *Phys. Rev. B*, 2018, **98**, 245148.
9 A. J. Friedman, S. Gopalakrishnan and R. Vasseur, Integrable Many-Body Quantum Floquet-Thouless Pumps, *Phys. Rev. Lett.*, 2019, **123**, 170603.
10 M. Taherinejad, K. F. Garrity and D. Vanderbilt, Wannier Center Sheets in Topological Insulators, *Phys. Rev. B: Condens. Matter Mater. Phys.*, 2014, **89**, 115102.
11 R. Li and M. Fleischhauer, Finite-Size Corrections to Quantized Particle Transport in Topological Charge Pumps, *Phys. Rev. B*, 2017, **96**, 085444.
12 M. J. Rice and E. J. Mele, Elementary Excitations of a Linearly Conjugated Diatomic Polymer, *Phys. Rev. Lett.*, 1982, **49**, 1455–1459.
13 L. Privitera, A. Russomanno, R. Citro and G. E. Santoro, Nonadiabatic Breaking of Topological Pumping, *Phys. Rev. Lett.*, 2018, **120**, 106601.
14 Y. Kuno, Non-Adiabatic Extension of the Zak Phase and Charge Pumping in the Rice–Mele Model, *Eur. Phys. J. B*, 2019, **92**, 195.
15 Z. Fedorova, H. Qiu, S. Linden and J. Kroha, Topological Transport Quantization by Dissipation in Fast Thouless Pumps, CLEO: QELS_Fundamental Science, *Opt. Soc. Am.*, 2020, FM2A.3.
16 T. Oka and S. Kitamura, Floquet Engineering of Quantum Materials, *Annu. Rev. Condens. Matter Phys.*, 2019, **10**, 387–408.
17 M. S. Rudner and N. H. Lindner, Band Structure Engineering and Non-Equilibrium Dynamics in Floquet Topological Insulators, *Nat. Rev. Phys.*, 2020, **2**, 229–244.
18 J. F. Khoury and L. M. Schoop, Chemical Bonds in Topological Materials, *Trends Chem.*, 2021, **3**, 700–715.
19 A. Martín Pendás, J. Contreras-García, F. Pinilla, J. D. Mella, C. Cardenas and F. Muñoz, A Chemical Theory of Topological Insulators, *Chem. Commun.*, 2019, **55**, 12281–12287.
20 A. Castro, U. De Giovannini, S. A. Sato, H. Huebener and A. Rubio, Floquet Engineering with Quantum Optimal Control Theory, *New J. Phys.*, 2023, **25**, 043023.
21 G. E. Topp, G. Jotzu, J. W. McIver, L. Xian, A. Rubio and M. A. Sentef, Topological Floquet Engineering of Twisted Bilayer Graphene, *Phys. Rev. Res.*, 2019, **1**, 023031.
22 R. Zhou, D. C. Yost and Y. Kanai, First-Principles Demonstration of Nonadiabatic Thouless Pumping of Electrons in a Molecular System, *J. Phys. Chem. Lett.*, 2021, **12**, 4496–4503.
23 R. Zhou and Y. Kanai, Dynamical Transition Orbitals: A Particle–Hole Description in Real-Time Tddft Dynamics, *J. Chem. Phys.*, 2021, **154**, 054107.
24 R. Zhou and Y. Kanai, Molecular Control of Floquet Topological Phase in Non-Adiabatic Thouless Pumping, *J. Phys. Chem. Lett.*, 2023, **14**, 8205–8212.
25 J. P. Perdew, K. Burke and M. Ernzerhof, Generalized Gradient Approximation Made Simple, *Phys. Rev. Lett.*, 1996, **77**, 3865–3868.
26 J. Sun, A. Ruzsinszky and J. P. Perdew, Strongly Constrained and Appropriately Normed Semilocal Density Functional, *Phys. Rev. Lett.*, 2015, **115**, 036402.
27 C. Adamo and V. Barone, Toward Reliable Density Functional Methods without Adjustable Parameters: The Pbe0 Model, *J. Chem. Phys.*, 1999, **110**, 6158–6170.
28 J. Ashkenazi, W. Pickett, H. Krakauer, C. Wang, B. Klein and S. Chubb, Ground State of Trans-Polyacetylene and the Peierls Mechanism, *Phys. Rev. Lett.*, 1989, **62**, 2016.
29 K. Hui and J.-D. Chai, Scan-Based Hybrid and Double-Hybrid Density Functionals from Models without Fitted Parameters, *J. Chem. Phys.*, 2016, 144.
30 C. Yannoni and T. Clarke, Molecular Geometry of Cis-and Trans-Polyacetylene by Nutation Nmr Spectroscopy, *Phys. Rev. Lett.*, 1983, **51**, 1191.
31 I. Ciofini, C. Adamo and H. Chermette, Effect of Self-Interaction Error in the Evaluation of the Bond Length Alternation in Trans-Polyacetylene Using Density-Functional Theory, *J. Chem. Phys.*, 2005, **123**, 121102.
32 V. Blum, M. Rossi, S. Kokott and M. Scheffler, The Fhi-Aims Code: All-Electron, Ab Initio Materials Simulations Towards the Exascale, *arXiv*, 2022, preprint, arXiv:2208.12335, DOI: **10.48550/arXiv.2208.12335**.

Open Access Article. Published on 13 June 2025. Downloaded on 12/6/2025 9:53:45 AM. This article is licensed under a Creative Commons Attribution 3.0 Unported Licence.

33 V. Blum, R. Gehrke, F. Hanke, P. Havu, V. Havu, X. Ren, K. Reuter and M. Scheffler, Ab Initio Molecular Simulations with Numeric Atom-Centered Orbitals, *Comput. Phys. Commun.*, 2009, **180**, 2175–2196.
34 S. Nosé, A Unified Formulation of the Constant Temperature Molecular Dynamics Methods, *J. Chem. Phys.*, 1984, **81**, 511–519.
35 W. G. Hoover, Canonical Dynamics: Equilibrium Phase-Space Distributions, *Phys. Rev. A*, 1985, **31**, 1695.
36 H. Shirakawa and S. Ikeda, Infrared Spectra of Poly (Acetylene), *Polym. J.*, 1971, **2**, 231–244.
37 E. Runge and E. K. U. Gross, Density-Functional Theory for Time-Dependent Systems, *Phys. Rev. Lett.*, 1984, **52**, 997–1000.
38 K. Yabana and G. F. Bertsch, Time-Dependent Local-Density Approximation in Real Time, *Phys. Rev. B: Condens. Matter Mater. Phys.*, 1996, **54**, 4484–4487.
39 J. Xu, T. E. Carney, R. Zhou, C. Shepard and Y. Kanai, Real-Time Time-Dependent Density Functional Theory for Simulating Nonequilibrium Electron Dynamics, *J. Am. Chem. Soc.*, 2024, **146**, 5011–5029.
40 A. Horsfield, M. Finnis, M. Foulkes, J. LePage, D. Mason, C. Race, A. Sutton, D. Bowler, A. Fisher and R. Miranda, Correlated Electron-Ion Dynamics in Metallic Systems, *Comput. Mater. Sci.*, 2008, **44**, 16–20.
41 I. Loaiza and A. F. Izmaylov, On the Breakdown of the Ehrenfest Method for Molecular Dynamics on Surfaces, *J. Chem. Phys.*, 2018, **149**, 214101.
42 A. Schleife, E. W. Draeger, V. M. Anisimov, A. A. Correa and Y. Kanai, Quantum Dynamics Simulation of Electrons in Materials on High-Performance Computers, *Comput. Sci. Eng.*, 2014, **16**, 54–60.
43 E. Draeger and F. Gygi, *Qbox Code, Qb@ Ll Version*, Lawrence Livermore National Laboratory, 2017.
44 C. Shepard, R. Zhou, D. C. Yost, Y. Yao and Y. Kanai, Simulating Electronic Excitation and Dynamics with Real-Time Propagation Approach to Tddft within Plane-Wave Pseudopotential Formulation, *J. Chem. Phys.*, 2021, **155**, 100901.
45 A. Kononov, C.-W. Lee, T. P. dos Santos, B. Robinson, Y. Yao, Y. Yao, X. Andrade, A. D. Baczewski, E. Constantinescu and A. A. Correa, Electron Dynamics in Extended Systems within Real-Time Time-Dependent Density-Functional Theory, *MRS Commun.*, 2022, **12**, 1002–1014.
46 C. Shepard, R. Zhou, J. Bost, T. E. Carney, Y. Yao and Y. Kanai, Efficient Exact Exchange Using Wannier Functions and Other Related Developments in Planewave-Pseudopotential Implementation of Rt-Tddft, *J. Chem. Phys.*, 2024, **161**, 024111.
47 G. Francois, Architecture of Qbox: A Scalable First-Principles Molecular Dynamics Code, *IBM J. Res. Dev.*, 2008, **52**, 137–144.
48 A. Schleife, E. W. Draeger, Y. Kanai and A. A. Correa, Plane-Wave Pseudopotential Implementation of Explicit Integrators for Time-Dependent Kohn-Sham Equations in Large-Scale Simulations, *J. Chem. Phys.*, 2012, **137**, 22A546.
49 D. R. Hamann, M. Schlüter and C. Chiang, Norm-Conserving Pseudopotentials, *Phys. Rev. Lett.*, 1979, **43**, 1494–1497.
50 D. Vanderbilt, Optimally Smooth Norm-Conserving Pseudopotentials, *Phys. Rev. B: Condens. Matter Mater. Phys.*, 1985, **32**, 8412–8415.
51 A. Castro, M. A. Marques and A. Rubio, Propagators for the Time-Dependent Kohn–Sham Equations, *J. Chem. Phys.*, 2004, **121**, 3425–3433.
52 D. C. Yost, Y. Yao and Y. Kanai, Propagation of Maximally Localized Wannier Functions in Real-Time Tddft, *J. Chem. Phys.*, 2019, **150**, 194113.
53 R. Resta, Quantum-Mechanical Position Operator in Extended Systems, *Phys. Rev. Lett.*, 1998, **80**, 1800.
54 M. Nakagawa, R.-J. Slager, S. Higashikawa and T. Oka, Wannier Representation of Floquet Topological States, *Phys. Rev. B*, 2020, **101**, 075108.
55 D. Vanderbilt, Berry Phases in Electronic Structure Theory: Electric Polarization, *Orbital Magnetization and Topological Insulators*, Cambridge University Press, Cambridge, 2018.
56 C. A. Ullrich, Time-Dependent Density-Functional Theory, *Concepts and Applications*, Oxford Graduate Texts, 2011.
57 M. A. Marques and E. K. Gross, Time-Dependent Density Functional Theory, *Annu. Rev. Phys. Chem.*, 2004, **55**, 427–455.
58 J.-L. Bredas, Relationship between Band Gap and Bond Length Alternation in Organic Conjugated Polymers, *J. Chem. Phys.*, 1985, **82**, 3808–3811.
59 D. Jacquemin and C. Adamo, Bond Length Alternation of Conjugated Oligomers: Wave Function and Dft Benchmarks, *J. Chem. Theory Comput.*, 2011, **7**, 369–376.
60 S. Yang and M. Kertesz, Bond Length Alternation and Energy Band Gap of Polyyne, *J. Phys. Chem. A*, 2006, **110**, 9771–9774.
61 R. L. Gieseking, C. Risko and J.-L. Bredas, Distinguishing the Effects of Bond-Length Alternation Versus Bond-Order Alternation on the Nonlinear Optical Properties of Π-Conjugated Chromophores, *J. Phys. Chem. Lett.*, 2015, **6**, 2158–2162.
62 D. Jacquemin, A. Femenias, H. Chermette, I. Ciofini, C. Adamo, J.-M. André and E. A. Perpète, Assessment of Several Hybrid Dft Functionals for the Evaluation of Bond Length Alternation of Increasingly Long Oligomers, *J. Phys. Chem. A*, 2006, **110**, 5952–5959.
63 J. K. Asbóth, L. Oroszlány, A. Pályi, J. K. Asbóth, L. Oroszlány and A. Pályi, *The Su-Schrieffer-Heeger (Ssh) Model*, *A Short Course on Topological Insulators: Band Structure and Edge States in One and Two Dimensions*, 2016, pp. 1–22.